

Evaluation of brushless DC motor structure design for the electric impact using 3-D finite element analysis

M. Senthil Raja, B. Geethalakshmi

Department of Electrical and Electronics Engineering, Puducherry Technological University, Puducherry, India.

Article Info

Article history:

Received Dec 13, 2021

Revised Jan 27, 2022

Accepted Feb 13, 2022

Keywords:

BLDC

Design procedure

Finite element analysis

Magnetic circuit

Torque density

ABSTRACT

In this article, an analytical model is deployed to optimize and design an interior permanent magnet brushless DC motor (IPMBLDC motor) when compared to theoretical structure of IPMBLDC. In this motor, assume air-gap of magnet assembly, distribution of flux density coefficient, selection of functional point in the permanent magnet, Torque density, and permanent magnet dimension compares with air-gap were deployed in an ideal design model. An equivalent circuit of magnetic field was improved and compare with the total flux density distribution and the torque density efficiency is based on initial ideal design factors. In finite element of MAXWELL 3D method, an electromagnetic field is investigated and used to verify an advanced equivalent circuit of magnetic field and improve the IPMBLDC motor factors. Finally, simulation results of IPMBLDC motor are verify and compare with ideal factors of IPMBLDC motor.

This is an open access article under the [CC BY-SA](https://creativecommons.org/licenses/by-sa/4.0/) license.



Corresponding Author:

M. Senthil Raja

Department of Electrical and Electronics Engineering, Puducherry Technological University

Puducherry 605014, India

Email: senthil.muthappa81@gmail.com

1. INTRODUCTION

Brushless direct current (BLDC) motors are one of the popular applications in industrial sector. In particular, this motor is used to control the servo motor systems and its electrical equipment because of its robustness, high efficiency, produces high torque for volume capacity ratio (VCR), and simplicity [1], [2]. The BLDC motor is studied for diverse energy levels at diverse applications. In order to get the parameters in BLDC motor, deploy Computer Aided tools but this tool takes long time to get this parameter in BLDC motor. Hence, in this article, we have introduced an Evaluation and tested system model to get the original parameters while designing BLDC motor. To optimize original parameters in BLDC motor, use MAXWELL 3-D FEM (finite element method) [3].

The effect of electrical motor is not working with model test continuously since it needs high consistency, low cost, small in size, high pull-out torque to load and to activate in manufacture in industrial sector [4]. In this article, the angle which is present in the lower torque is chosen by rated speed and its speed while designing the motor in optimized manner. Hence, this optimized design is used to enhance the potential of overload while handling this design efficiently and get large torque during short time. Hence, this produces the BLDC motor design in regular manner and also reduces design time [5]. In the account of design consideration, the initial design parameters are magnet assembly gap, rotor saturation, Assumed flux leakage coefficient, rotor saturation, and permanent magnet [6].

Interior permanent magnet brushless DC (IPMBLDC) electric motor is the main type of these motors, constructed with the permanent magnets inserted into the rotor core [7]. The pathway of leakage in an interior permanent magnet motor comprises a saturable magnetic reaction which creates the coefficient

variable for flux leakage [8]. This article determines and to test the design in the interior portion of permanent magnet brushless DC motor and it is used to concentrate the windings and also, apply in electric parameters in this motor. The equivalent magnetic circuit of the IPMBLDC motor is to analyze the coefficient of flux and working selected point of a permanent magnet based on the design output parameters. The MAXWELL 3D FEM is deployed to validate the equivalent circuit of magnetic field and optimize the IPMBLDC motor design. To validate the design, the experimental responses are shown.

2. MOTOR DESIGN PROCEDURE

The interior permanent magnet BLDC motor design procedure is very difficult when compare with other motor [9]. In IPMBLDC motor, the leakage which is produce in magnetic flux and its path generally comprises saturable magnetic circuits. The BLDC motor of 24 slot IPMBLDC design procedure as sown in Figure 1. The flux leakage coefficient ϕL and the operational point in the permanent magnet ψm are deployed for the first design process in IPMBLDC motor. The metric value for ϕL and ψm are assumed after selected parameters are evaluated roughly based on our equivalent circuits. We offer the primary design size of the IPMBLDC motor, system model, and a small torque angle value value when compare to legacy designs by the rated load. Therefore, we get greater overloading handling capacity and enhanced total efficiency. Then, to verify the design process and parameters, analyse the finite element and simulate FEM.

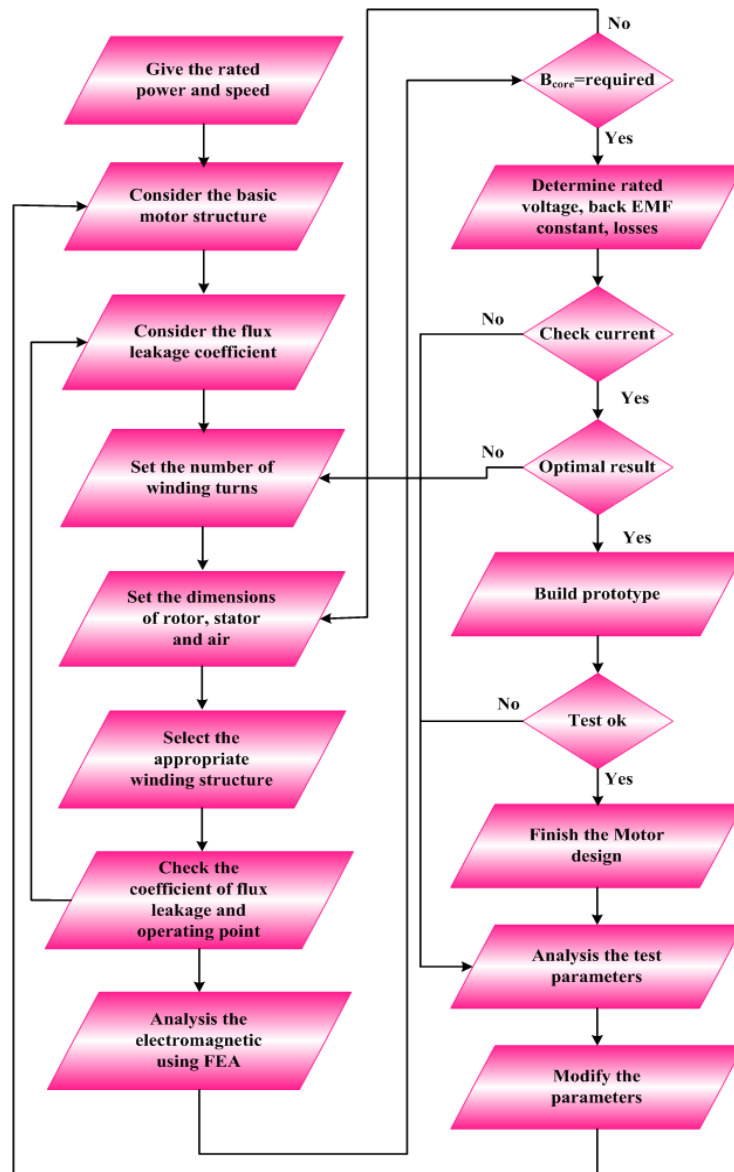


Figure 1. 24 slot IPMBLDC design procedure

In Figure 2, shows the configuration of 24 slot IPMBLDC motor. The loop of core flux flows via the magnet, yoke in stator, air-gap, winding in stator, tooth in stator, and yoke in rotor. The flux linkages taking in to consideration for permanent magnet, the IPMBLDC motor equivalent magnetic circuits and these two combined with half-pole pair to assume the equilibrium for this motor.

$$R_l = \frac{R_s}{4} + R_{st} + R_{ag} + R_{ra} + R_{rb} \tag{1}$$

Where R_l is the total reluctance of air gap; R_s is the reluctance of stator yoke; R_{st} is the reluctance of stator tooth; R_{ag} is the reluctance of Air gap; R_{ra} is the rotor reluctance above the magnet; R_{rb} is the rotor reluctance below the magnet.

The magnet ending flux leakage reluctances can be expressed as (2).

$$R\sigma = \frac{d_\sigma}{\mu_0 A_\sigma} \tag{2}$$

Where d_σ is the magnet distance and the yoke channel A_σ is the area of the cross section in the air gap. The magnetic reluctance can be expressed as (3).

$$R_{m0} = \frac{h_m}{\mu_0 \mu_r A_m} \tag{3}$$

Where h_m is the permanent magnet length. A_m is the area of the cross section in the magnet. The summation of magnet ending flux leakage reluctances and reluctance of magnet can be expressed as (4).

$$R_0 = R_0 + R_{m0} \tag{4}$$

To calculate the consistency of the certain operation point and the coefficient of the flux leakage, it is essential to analyze the equivalent of the magnet circuit [10] as shown in Figure 3, we consider the density of web flux in the magnet is 1.8 tesla. Hence, the leakage of the flux in magnet ϕL is obtained. The density of flux in the magnet intensity is limited to 2 Tesla.

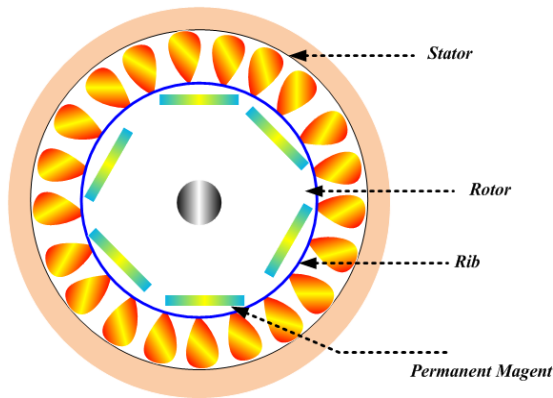


Figure 2. 24 slot IPMBLDC motor configuration

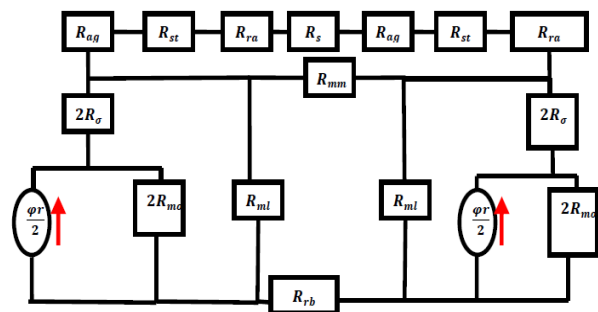


Figure 3. Magnetic equivalent circuit

3. THE DESIGN AND CALCULATION OF BLDC MOTOR

3.1. Dimension of the permanent magnet

When the air-gap dimension is obtained, the (5) and (6) can be used based on [10] to conclude the dimension of the permanent magnet. Assumed flux leakage coefficient and selected permanent magnet operating point are used in the equations.

$$h_m = \frac{K_s K_\alpha \alpha_m}{(1 - \alpha_m) \phi_L} g \tag{5}$$

Where h_m is the permanent magnet length; g is the air gap length; K_s is the motor saturation factor; K_α is the rotor structure factor. The IPMBLDC motor air gap flux produces square waveform, hence the metric rate of the pole is coefficient must be greater for sufficient case see in [11]. The permanent magnetic width can be expressed as (6).

$$b_m = \frac{2\phi_L B_g p k \tau_1}{\pi \alpha_m B_r K_\phi} \quad (6)$$

Where B_g , is the peak value of air gap in fundamental wave; K_ϕ is the air gap flux waveform factor. In IPMBLDC motor, the coefficient for pole is formulated in (6). The metric value of the saturation factor in motor varies between 1 and 1.3. The value of the structure factor for rotor between 0.7 and 1.

The permanent magnet material B-H curve is shown in Figure 4(a) (see Appendix). The permanent magnet operational point is related with motor energy. B_m is the flux density and H_m is the magnetizing force in the magnet. There are two lines in the operational point of the permanent magnet known as load and device line. The line in the load is mentioning the line via the starting point to the operational point and the device line is distinct as an ideal demagnetization curve [12]. The ideal IPMBLDC motor air gap flux waveform is square. Some derivation, the permanent magnet flux density is formulated as:

$$H_m = -(1 - \psi_m) H_c \quad (7)$$

$$B_m = -(\mu_0 H_m) \quad (8)$$

$$P_c = (A_g/g)/(A_m/dm) \quad (9)$$

Where P_c is permanence coefficient; A_g is air-gap area; g is air-gap length; A_m is cross-sectional area; dm is the distance between the magnet; ψ_m is called the operating point of a permanent magnet.

The simulated B-H curve of the permanent magnet material is shown in Figure 4(b) (see Appendix). In this experiment we have chosen carbon steel. It is a normal carbon steel with 0.10 percentage of carbon content. We achieve the selection of the power in maximum level is $\psi_m=0.5$. In order to overcome the demagnetization effect, we always select an operating point larger than 0.5. In the proposal, the operating point between 0.5 and 1 is chosen [13]. To find out the air-gap of the magnetic field from the rotor of PM. We have used as an expansion of fourier series; the air-gap of flux density in magnetic field is given by:

$$B_{rh} = \frac{2}{2\pi} \left[\int_{-\frac{\rho_{PM}}{2}}^{\frac{\rho_{PM}}{2}} B_m \cos(h\theta) + \int_{\pi-\frac{\rho_{PM}}{2}}^{\pi+\frac{\rho_{PM}}{2}} -B_m \cos(h\theta) \right] \quad (10)$$

$$B_{rh} = \frac{4 \sin(h \frac{\rho_{PM}}{2}) B_m}{\pi h} \quad (11)$$

$$K_{ph} = \sin(h \frac{P_m}{2}) \quad (12)$$

$$B_{r,pk} = \frac{4}{\pi} \sin(\frac{\rho_{PM}}{2}) B_m \quad (13)$$

Where K_{ph} is the pitch factor of h th harmonic; B_{rh} is the air-gap flux density; $B_{r,pk}$ is the peak air-gap flux density.

4. PERFORMANCE INVESTIGATION

To validate the design parameters and magnetic circuit model, the 3D Finite element investigation has been used. We consider the density of the flux is constrained from 1.6 and 1.8 Tesla. For this IPMBLDC motor, Magnet 3D is deployed to estimate and improve the original factors are obtained from the equation for motor design. The design purpose is to decrease the ripples which are present in the torque and enhance the efficiency. Certain factors namely air-gap length, magnet length, and so on will be a little modified to get improved performance [14]. The dimensions of the IPMBLDC motor model are shown in Table 1.

Table 1. Dimension of the motor model

S.L.	Model in motor	Range
1	The slots/pole Numbers	12/4
2	Outer diameter/mm in Stator	48
3	Inner diameter/mm in Stator	24
4	length/mm for Air-gap	0.2
5	Length/mm in Magnet	9
6	Voltage in volts	200
7	Current in Amps	1
8	Power in watts	200
9	Speed in rpm	2500
10	Torque in N-m	1

In Pulsating, torque is the relation impacts between the permanent magnet field in the rotor and the teeth of the stator pole [15]. It builds a torque pulsating that does not contribute to the effective of the total torque [16]. The flux distribution waveform angle and torque characteristics for the IPMBLDC are shown in Figure 5 and Figure 6. The ampere-flux distribution of the stator residue is constant and predetermined in space for a fixed commutation interval as the magnet rotates the previous period, produce a linear phase difference variation of flux-linkages, and from flat-top back-waveform for EMF [17], [18]. To get high torque density, modification done in stator concentrated windings and rotor dimensions are used [19], so the value of torque ripples and motor efficiency is suitable for 12-slots, 4-pole motor. The speed characteristics of the IPMBLDC motor model are shown in Figure 7. The speed versus torque plot of the IPMBLDC motor model is shown in Figure 8. The torque increases, the motor speed is decreased. The plot shows that the design model has around close to the theoretical existing motor characteristics graph. Detailed simulated relationship between torque, flux density, and speed is shown in Table 2.

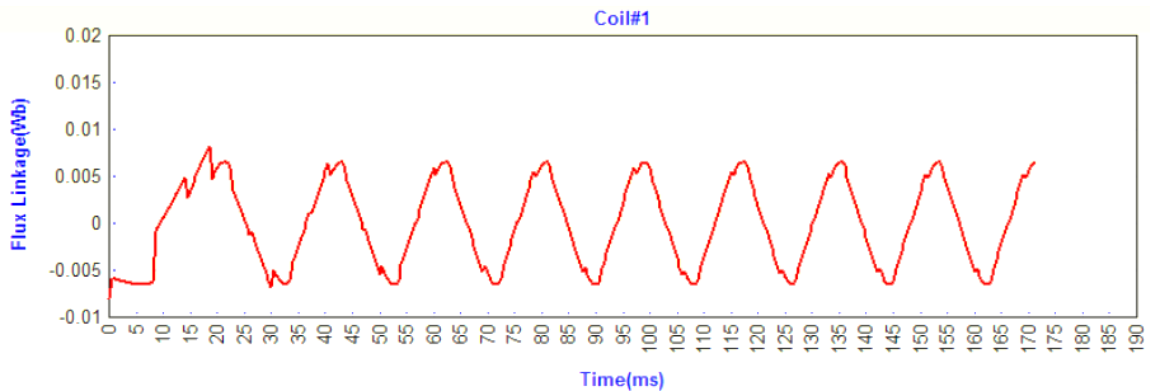


Figure 5. Flux density distribution

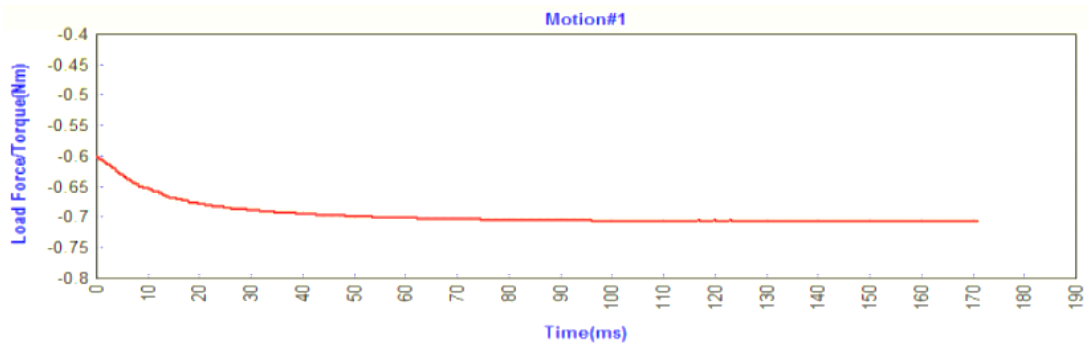


Figure 6. Torque characteristics

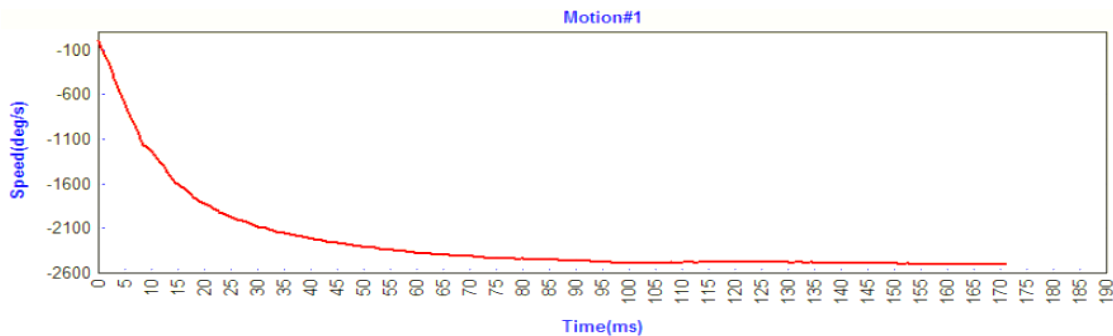


Figure 7. Speed characteristics

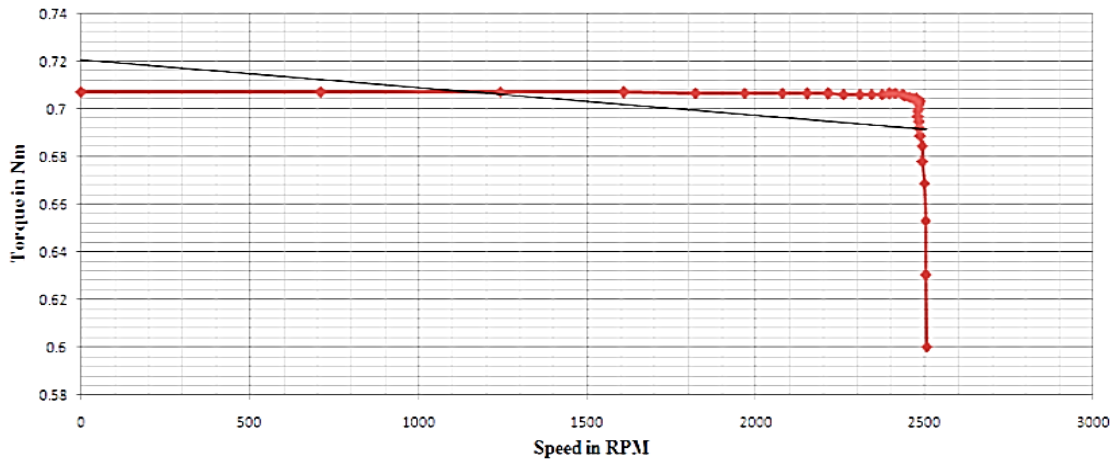


Figure 8. Speed vs torque characteristics

Table 2. Detailed simulated relationship between torque, flux density, and speed are shown

Time in sec.	Flux Linkage	Speed(deg/sec)	Load Force/Torque(Nm)
0	-0.008011516828	0	-0.6
5	-0.006536902708	-710.6986868	-0.6303898785
10	0.0005355561372	-1242.931520	-0.6531484561
15	0.003531455894	-1607.503179	-0.668737746
20	0.005934708220	-1822.05293	-0.6779120158
25	0.000345140740	-1966.694286	-0.6840969621
30	-0.006862879536	-2078.011213	-0.6888569370
35	-0.002448606938	-2151.676149	-0.6920068914
40	0.005540622231	-2215.866840	-0.6947517217
45	0.002907926839	-2261.638092	-0.6967089264
50	-0.005417490002	-2308.086414	-0.6986950830
55	-0.002690250688	-2343.616719	-0.7002143789
60	0.005971689114	-2376.527811	-0.7016216759
65	0.00190826119	-2395.715475	-0.7024421513
70	-0.005346391726	-2414.224014	-0.7032335869
75	-0.000732794433	-2434.628720	-0.7041061037
80	0.006230476736	-2443.034874	-0.7044655556
85	-0.000324799638	-2456.101107	-0.7050242751
90	-0.006544184562	-2464.358617	-0.7053773709
95	0.002230922776	-2475.212666	-0.7058414962
100	0.00592900262	-2488.032278	-0.7063896701
105	-0.003704002075	-2485.11041	-0.7062647297
110	-0.003651447474	-2483.060521	-0.7061770750
115	0.00543777656	-2481.82806	-0.7061243745
120	0.001876431442	-2479.914360	-0.7060425433
125	-0.005751353033	-2480.390204	-0.7060628907
130	-0.000106910481	-2483.845997	-0.7062106623
135	0.006525068983	-2484.412592	-0.7062348903
140	-0.001449741492	-2488.078118	-0.7063916302
145	-0.006225249296	-2493.286151	-0.7066143287
150	0.003320757915	-2495.135609	-0.7066934126
155	0.003953507962	-2499.779089	-0.7068919704
160	-0.005128059792	-2504.419074	-0.7070903787
165	-0.002124128813	-2505.476122	-0.7071355787
170	0.005605705254	-2507.624183	-0.7072274311

The analysis of the fast fourier transform (FFT) in flux distribution of air gap is shown in Figure 9. Only odd harmonics ripples are appeared but even harmonics ripples are disappeared, which results that the ripples of flux density distribution in the air-gap are in excellent condition [20]. Measuring the torque of the motor is very difficult. It requires costly equipment. So we suggest calculating the efficiency of the motor. It is calculated as the ratio of mechanical output power to electrical input power.

$$E = \frac{P_{out}}{P_{in}} \tag{14}$$

$$P_{out} = P_{in} \times E \quad (15)$$

Output mechanical power of the motor is calculated by:

$$P_{out} = T \times \omega \quad (16)$$

$$\omega = rpm \times \frac{2\pi}{60} \quad (17)$$

$$P_{out} = T \times rpm \times \frac{2\pi}{60} \quad (18)$$

$$P_{in} \times E = T \times rpm \times \frac{2\pi}{60} \quad (19)$$

$$I \times V \times E = T \times rpm \times \frac{2\pi}{60} \quad (20)$$

$$T = \frac{I \times V \times E \times 60}{rpm \times 2\pi} \quad (21)$$

Efficiency is chosen between zero to maximum; in our simulation below 2500 rpm is optimal speed for calculations, it is used 100% efficiency ($E = 1$).

$$I = 1 \text{ A}, V = 200 \text{ V}, E = 1 \text{ and } rpm = 2500$$

$$T = (1 \times 200 \times 1 \times 60) / (2500 \times 2 \times 3.14) = 0.76 \text{ N-m}$$

Where P_{in} is the input power in watts (W); I is the current measured in ampere (A); V is the voltage measured in volts (V); T is the Torque in Newton-meter (N-m); ω is the angular speed in radian per second. The torque efficiency is based on equation (21). For the simulation efficiency is 93%, some mechanical losses are neglected and the parameter is chosen the very nearest and rounded value, this is the reason simulation efficiency is 7% lower than the theoretical efficiency.

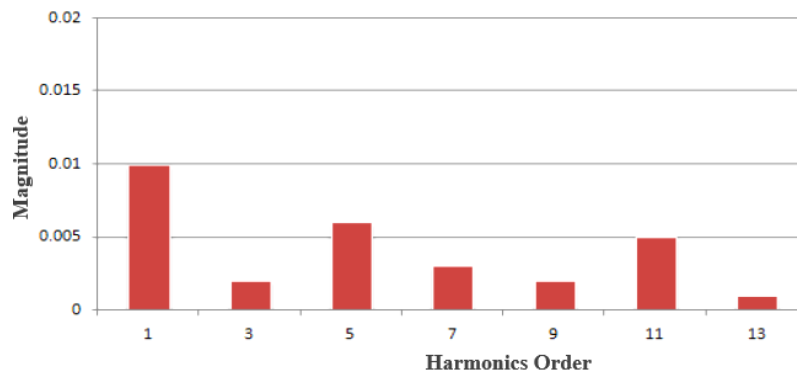


Figure 9. Fast fourier transform analysis

5. CONCLUSION

In this paper, we compared to design the IPMBLDC motor using 3D-Finite element analysis and the structure of the theoretical design for electrical effect determination of IPMBLDC. The representation of the magnetic circuit has been developed to evaluate the permanent magnet dimension, the operational point of a permanent magnet, coefficient of flux linkage, and torque efficiency. The theoretical design has been compared and confirmed using MAXWELL 3D analysis based on FEM. Finally, torque efficiency is compared with the theoretical design structure and analytical method of FEM. The theoretical calculated torque density is 0.76(N-m) and simulated torque density is 0.70(N-m). The simulated torque efficiency of 93% is very close to the theoretical torque efficiency. Therefore, the MAXWELL 3D analysis tool is most suitable for optimized and analyzing structure and evaluation of electrical impact

ACKNOWLEDGEMENTS

Authors gratefully acknowledge the support of Muthukrishna Babu, Scientist from National Institute of Ocean Technology (NIOT) India, for their valuable suggestions and software support.

APPENDIX

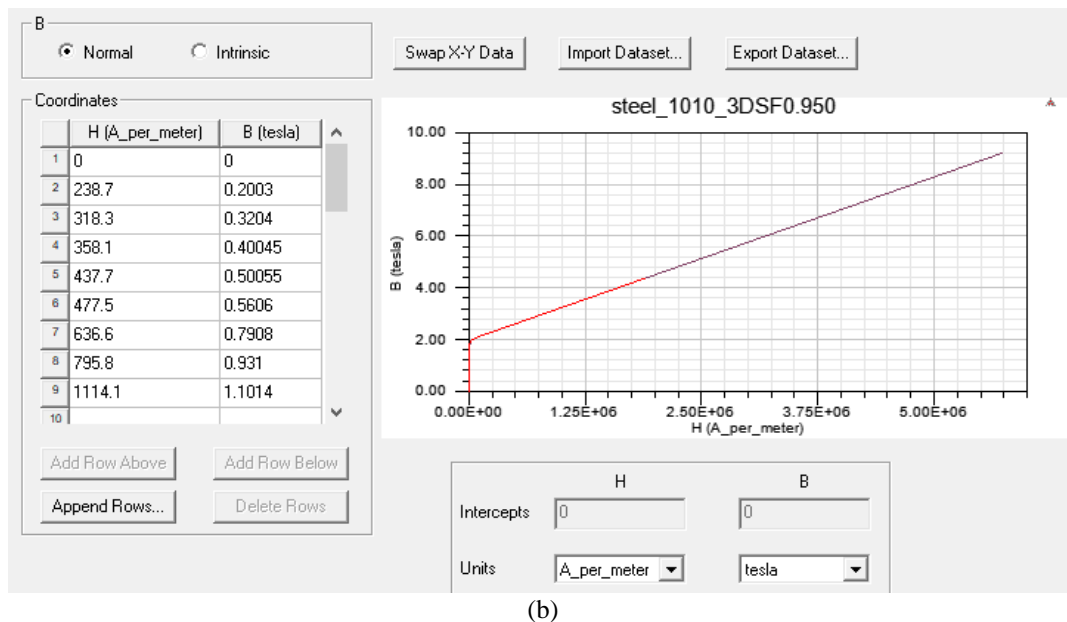
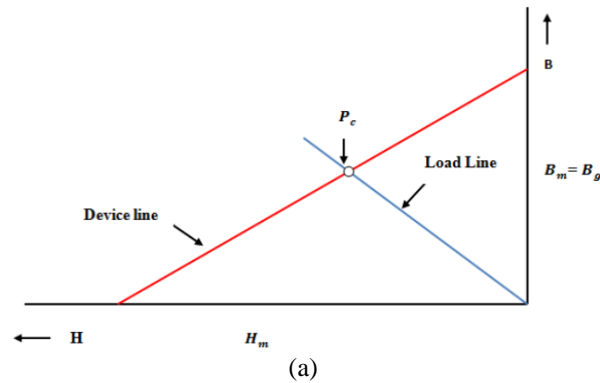


Figure 4. The permanent magnet material: (a) B-H curve of the permanent magnet material and (b) simulated B-H curve of the permanent magnet material




REFERENCES

- [1] H.-S. Seol, D.-W. Kang, H.-W. Jun, J. Lim, and J. Lee, "Design of Winding Changeable BLDC Motor Considering Demagnetization in Winding Change Section," *IEEE Trans. Magn.*, vol. 53, no. 11, pp. 1–5, Nov. 2017, doi: 10.1109/TMAG.2017.2695890.
- [2] M. S. Raja and B. Geethalakshmi, "Analysis and Implementation of a High Boost Ratio DC-DC Converter for Minimizing Commutation Torque Ripple in Brushless DC Motor," *Int. J. Power Electron. Drive Syst.*, vol. 7, no. 2, p. 583, Jun. 2016, doi: 10.11591/ijpeds.v7.i2.pp583-600.
- [3] H. Kim, Y.-M. You, and B. Kwon, "Rotor Shape Optimization of Interior Permanent Magnet BLDC Motor According to Magnetization Direction," *IEEE Trans. Magn.*, vol. 49, no. 5, pp. 2193–2196, May 2013, doi: 10.1109/TMAG.2013.2242056.
- [4] C. He, T. Wu, W. Wu, L. Chow, J. Harms, and D. R. Taylor, "Design, analysis and experiment of a high efficiency permanent magnet truck alternator," in *IECON 2017 - 43rd Annual Conference of the IEEE Industrial Electronics Society*, Oct. 2017, pp. 1905–1910, doi: 10.1109/IECON.2017.8216322.
- [5] P. Mukherjee, S. Paitandi, and M. Sengupta, "Comparative analytical and experimental study of fabricated identical surface and interior permanent magnet BLDC motor prototypes," *Sādhanā*, vol. 45, no. 1, p. 26, Dec. 2020, doi: 10.1007/s12046-019-1264-0.
- [6] S.-M. Jang, H.-I. Park, J.-Y. Choi, K.-J. Ko, and S.-H. Lee, "Magnet Pole Shape Design of Permanent Magnet Machine for Minimization of Torque Ripple Based on Electromagnetic Field Theory," *IEEE Trans. Magn.*, vol. 47, no. 10, pp. 3586–3589, Oct. 2011, doi: 10.1109/TMAG.2011.2151846.




- [7] Y.-S. Lee, K.-T. Kim, and J. Hur, "Finite-Element Analysis of the Demagnetization of IPM-Type BLDC Motor With Stator Turn Fault," *IEEE Trans. Magn.*, vol. 50, no. 2, pp. 889–892, Feb. 2014, doi: 10.1109/TMAG.2013.2283498.
- [8] C. He and T. Wu, "Design and analysis of a V-type fractional-slots IPMSM with distributed winding for electric vehicles," in *2016 XXII International Conference on Electrical Machines (ICEM)*, Sep. 2016, pp. 1459–1465. doi: 10.1109/ICELMACH.2016.7732716.
- [9] K.-H. Shin, J.-Y. Choi, and H.-W. Cho, "Characteristic Analysis of Interior Permanent-Magnet Synchronous Machine With Fractional-Slot Concentrated Winding Considering Nonlinear Magnetic Saturation," *IEEE Trans. Appl. Supercond.*, vol. 26, no. 4, pp. 1–4, Jun. 2016, doi: 10.1109/TASC.2016.2514340.
- [10] T. Wellawatta, J. Park, H.-M. Kim, and J. Hur, "New equivalent circuit of the IPM-type BLDC motor for calculation of shaft voltage by considering electric and magnetic fields," in *2015 IEEE Energy Conversion Congress and Exposition (ECCE)*, Sep. 2015, pp. 1872–1877. doi: 10.1109/ECCE.2015.7309923.
- [11] S. Sashidhar and B. G. Fernandes, "Braking Torque Due to Cross Magnetization in Unsaturated IPM BLDC Machines and Its Mitigation," *IEEE Trans. Magn.*, vol. 53, no. 1, pp. 1–9, Jan. 2017, doi: 10.1109/TMAG.2016.2618343.
- [12] M. H. Nagrial, J. Rizk, and A. Hellany, "Design and performance of interior permanent magnet motors with saturating magnetic bridge," in *2009 IEEE International Electric Machines and Drives Conference*, May 2009, pp. 922–927. doi: 10.1109/IEMDC.2009.5075314.
- [13] C. He and T. Wu, "Permanent Magnet Brushless DC Motor and Mechanical Structure Design for the Electric Impact Wrench System," *Energies*, vol. 11, no. 6, p. 1360, May 2018, doi: 10.3390/en11061360.
- [14] S.-K. Lee, G.-H. Kang, J. Hur, and B.-W. Kim, "Stator and Rotor Shape Designs of Interior Permanent Magnet Type Brushless DC Motor for Reducing Torque Fluctuation," *IEEE Trans. Magn.*, vol. 48, no. 11, pp. 4662–4665, Nov. 2012, doi: 10.1109/TMAG.2012.2201455.
- [15] H. Kim and B. Kwon, "Optimal design of motor shape and magnetisation direction to obtain vibration reduction and average torque improvement in IPM BLDC motor," *IET Electr. Power Appl.*, vol. 11, no. 3, pp. 378–385, Mar. 2017, doi: 10.1049/iet-epa.2016.0618.
- [16] R. Nasiri-Zarandi, M. Mirsalim, and A. Cavagnino, "Analysis, Optimization, and Prototyping of a Brushless DC Limited-Angle Torque-Motor With Segmented Rotor Pole Tip Structure," *IEEE Trans. Ind. Electron.*, vol. 62, no. 8, pp. 4985–4993, Aug. 2015, doi: 10.1109/TIE.2015.2402115.
- [17] Haibin Duan and Lu Gan, "Orthogonal Multiobjective Chemical Reaction Optimization Approach for the Brushless DC Motor Design," *IEEE Trans. Magn.*, vol. 51, no. 1, pp. 1–7, Jan. 2015, doi: 10.1109/TMAG.2014.2325797.
- [18] C. Ma, Q. Li, H. Lu, Y. Liu, and H. Gao, "Analytical model for armature reaction of outer rotor brushless permanent magnet DC motor," *IET Electr. Power Appl.*, vol. 12, no. 5, pp. 651–657, May 2018, doi: 10.1049/iet-epa.2017.0751.
- [19] M. S. Raja and B. Geethalakshmi, "Modified Rotor Material for Minimization of Torque Ripple for Interior Permanent Magnet BLDC motor," *Mater. Today Proc.*, vol. 5, no. 2, pp. 3639–3647, 2018, doi: 10.1016/j.matpr.2017.11.614.
- [20] G. Valente, L. Papini, A. Formentini, C. Gerada, and P. Zanchetta, "Radial force control of multisector permanent-magnet machines for vibration suppression," *IEEE Trans. Ind. Electron.*, vol. 65, no. 7, pp. 5395–5405, Jul. 2018, doi: 10.1109/TIE.2017.2780039.

BIOGRAPHIES OF AUTHORS



M. Senthil Raja    was born in Tamilnadu, India in 1981. He received B.E degree in Electronics & Communication Engineering from Anna University in 2005, the M.E degree in Power Electronics & Drives from Anna University in 2011. He is currently research scholar in Pondicherry University and Project Engineer SCADA system in Centre for Technology Development and Transfer (CTDT) in Anna University. He is an Associate Member of the Institution of Engineers (India). His research interests include power converter and electrical drives. He can be contacted at email: senthil.muthappa81@gmail.com.



B. Geethalakshmi    received the B.E (ECE) and M.E (Power Electronics and Drives) degree in 1996 and 1999 from Bharathidasan University respectively, and received Ph.D. degree in FACTS controllers from Pondicherry University in 2009. She is currently working as an Associate Professor in Electrical & Electronics Engineering department in Pondicherry Engineering College. Her current research interest comprises FACTS controller, power electronics, and motor drives. She can be contacted at email: bgeethalakshmi@pec.edu.